Relativistic Hartree-Fock-Bogoliubov model for deformed nuclei

Ebran, J.-P.; Khan, E.; Pena Arteaga, D.; Vretenar, Dario

Source / Izvornik: **Physical Review C - Nuclear Physics, 2011, 83**

Journal article, Published version
Rad u časopisu, Objavljena verzija rada (izdavačev PDF)

https://doi.org/10.1103/PhysRevC.83.064323

Permanent link / Trajna poveznica: https://urn.nsk.hr/urn:nbn:hr:217:338777

Relativistic Hartree-Fock-Bogoliubov model for deformed nuclei

J.-P. Ebran,[1] E. Khan,[1] D. Peña Arteaga,[1] and D. Vretenar[2]
[1]*Institut de Physique Nucléaire, Université Paris-Sud, IN2P3-CNRS, FR-91406 Orsay Cedex, France*
[2]*Physics Department, Faculty of Science, University of Zagreb, HR-10000 Zagreb, Croatia*
(Received 22 October 2010; revised manuscript received 13 May 2011; published 27 June 2011)

The relativistic Hartree-Fock-Bogoliubov model for axially deformed nuclei (RHFBz) is introduced. The model is based on an effective Lagrangian with density-dependent meson-nucleon couplings in the particle-hole channel, and the central part of the Gogny force is used in the pairing channel. The RHFBz quasiparticle equations are solved by expansion in the basis of a deformed harmonic oscillator. Illustrative RHFBz calculations are performed for carbon, neon, and magnesium isotopes. The effect of explicitly including the pion field is investigated for binding energies, deformation parameters, and charge radii and has an impact on the nuclei's shape.

DOI: 10.1103/PhysRevC.83.064323 PACS number(s): 24.10.Cn, 24.10.Jv, 21.60.Jz, 21.30.Fe

I. INTRODUCTION

Among the microscopic approaches to the nuclear many-body problem, nuclear energy density functionals (EDF) represent a tool of choice for the description of both static and dynamic properties of nuclei over the whole nuclide chart. EDFs subsum nucleonic short-range in-medium correlations, whereas static long-range correlations (deformation, pairing, etc.) are incorporated by allowing a single-determinant state to break the symmetries of the nuclear Hamiltonian [1]. A variety of structure phenomena in stable and exotic nuclei have successfully been described by EDFs based on the nonrelativistic Gogny and Skyrme [2] effective interactions, as well as on relativistic phenomenological Lagrangian densities [3]. There are significant advantages in using covariant functionals [4]. The most obvious is the natural inclusion of the nucleon spin degree of freedom and the resulting nuclear spin-orbit potential which emerges automatically with the empirical strength in a covariant formulation. The consistent treatment of large, isoscalar, Lorentz scalar, and vector self-energies provides a unique parametrization of time-odd components of the nuclear mean field [5], i.e., nucleon currents, which is absent in the nonrelativistic representation of the energy density functional. The empirical pseudospin symmetry in nuclear spectroscopy finds a natural explanation in terms of relativistic mean fields [6]. A covariant treatment of nuclear matter provides a distinction between scalar and four-vector nucleon self-energies, leading to a very natural saturation mechanism.

An example of a covariant EDF is known as the relativistic mean field (RMF) framework [3]. The corresponding effective Lagrangians provide a quantitative description of a variety of ground-state data (masses, charge radii, etc.). RMF, however, does not explicitly consider the Fock term. The exchange contributions are implicitly taken into account through the fit of model parameters to structure data. A more involved approach, the relativistic Hartree-Fock (RHF) theory [7], includes the exchange contributions explicitly. Early RHF models used to predict nuclei that were considerably underbound compared to experiment. The reason for this was the lack of a medium dependence in the corresponding effective nucleonic interaction [7]. The effect of the nuclear medium was first taken into account by adding self-interaction terms for the σ meson field [8]. Although some improvement was obtained, the RHF results were still not on the level of RMF model predictions. An explicit nucleon-density dependence of the nucleon-meson couplings was included in Ref. [9]. This brought significant improvement, so that current RHF models provide a quantitative description of nuclear properties with a similar accuracy as that of the standard RMF approach [10]. In particular, recent studies by Long *et al.* [9–12] and Liang *et al.* [13,14] have shown that, compared to the RMF approach, the explicit treatment of Fock terms can improve the description of nuclear matter and finite nuclei. Moreover, it explicitly takes into account the tensor contributions to the internucleon interaction generated by the exchange of the π and ρ mesons. These contributions have been found to play an important role in the description of the evolution of shell structures in the framework of the shell model [15]. The explicit treatment of exchange contributions in covariant EDF models enables the inclusion of the pion field, which contributes only via its Fock term, and the tensor ρ-nucleon coupling, which contributes predominantly in the exchange channel. The pion contribution is expected to improve the predicted evolution of shell structure [11], whereas the inclusion of the tensor ρ-nucleon coupling cures artificial shell gaps that arise in covariant EDF-based models [12].

Another benefit brought about by the explicit treatment of the Fock term deals with the random phase approximation (RPA) description of collective excitations. For example, the RHF + RPA approach provides a fully self-consistent description of charge-exchange excitations [13], in contrast to the RMF + RPA model in which additional terms have to be introduced [16].

When considering applications an important challenge for the framework of EDF is the systematic treatment of collective correlations related to restoration of broken symmetries and fluctuations in collective coordinates. A static nuclear EDF is characterized by symmetry breaking—translational, rotational, and particle number, and can only provide an approximate description of bulk ground-state properties. To

calculate excitation spectra and electromagnetic transition rates in individual nuclei, it is necessary to extend the self-consistent mean-field scheme to include correlations that arise from symmetry restoration and fluctuations around the mean-field minimum. RMF-based models have recently been developed that include the explicit treatment of collective correlations and have been employed in spectroscopic studies of a variety structure phenomena related to shell evolution [17].

The RHF framework has so far been limited to the description of spherical nuclei. In this work we consider an extension of this approach to deformed, axially symmetric nuclei, and introduce the relativistic Hartree-Fock-Bogoliubov model with density-dependent meson-nucleon couplings (RHFBz). In Sec. II the general formalism of the RHFBz model is presented. In Sec. III we present and discuss the first applications of the RHFBz model to ground-state properties of carbon, neon, and magnesium isotopes. To compare the results with those obtained with the standard relativistic Hartree-Bogoliubov (RHB) model [3], calculations are first performed without the inclusion of the pion field (PKO2 parametrization [18,19]). The effects induced by the pion field are analyzed in RHFBz calculations based on the PKO3 parameter set [18,19]. Finally, Sec. IV contains a short summary and discussion of possible future studies.

II. FORMALISM OF THE RHFBz MODEL

A. Energy density functional

1. Effective Lagrangian and equations of motion

The RHFBz approach is based on a phenomenological Lagrangian density formulated in terms of relevant degrees of freedom for nuclear structure, namely nucleons and mesons. Nucleons are treated as pointlike Dirac particles. The effective in-medium interaction between nucleons is described by meson exchange, whereas the Coulomb interaction between protons is taken into account by the electromagnetic 4 potential A^μ. The Lagrangian density reads

$$\begin{aligned}\mathcal{L} = \bar{\psi}\Big\{ & i\gamma^\mu\partial_\mu - M - g_\sigma(\rho_v)\sigma - g_\omega(\rho_v)\gamma_\mu\omega^\mu \\ & - g_\rho(\rho_v)\gamma_\mu\vec{\rho}\cdot\vec{\tau}^\mu - \frac{f_\pi(\rho_v)}{m_\pi}\gamma_5\gamma_\mu\partial^\mu\vec{\pi}\cdot\vec{\tau} \\ & - e\gamma_\mu A^\mu\frac{1-\tau_3}{2}\Big\}\psi + \frac{1}{2}\left(\partial_\mu\sigma\,\partial^\mu\sigma - m_\sigma^2\sigma^2\right) \\ & - \frac{1}{2}\left(\Omega_{\mu\nu}\Omega^{\mu\nu} - m_\omega^2\omega_\mu\omega^\mu\right) - \frac{1}{2}\left(\vec{\mathcal{R}}_{\mu\nu}\vec{\mathcal{R}}^{\mu\nu} - m_\rho^2\vec{\rho}_\mu\vec{\rho}^\mu\right) \\ & + \frac{1}{2}\left(\partial_\mu\vec{\pi}\,\partial^\mu\vec{\pi} - m_\pi^2\vec{\pi}^2\right) - \frac{1}{2}(\mathcal{F}_{\mu\nu}\mathcal{F}^{\mu\nu}). \end{aligned} \tag{1}$$

Vectors in isospin space are denoted by arrows, and boldface symbols will indicate vectors in ordinary three-dimensional space. The Dirac spinor ψ denotes the nucleon with mass M. m_σ, m_ω, m_ρ, and m_π are the masses of the σ meson, ω meson, ρ meson, and π meson, respectively. g_σ, g_ω, g_ρ, and f_π are the corresponding coupling constants for the mesons to the nucleon. $e^2/4\pi = 1/137.036$. The (density-dependent) coupling constants and meson masses are parameters, adjusted to reproduce nuclear matter properties and ground-state properties of finite nuclei. $\Omega^{\mu\nu}$, $\vec{R}^{\mu\nu}$, and $\mathcal{F}^{\mu\nu}$ are the field tensors of the vector fields ω, ρ, and of the photon [7]. A nucleon-density dependence of the meson-nucleon couplings accounts for medium polarization and three-body correlations [9,20,21]. The effective Lagrangian is, therefore, characterized by eight free parameters,

$$\begin{aligned} & m_\sigma,\ g_\sigma(\rho_{\rm sat}),\ b_\sigma,\ d_\sigma, \\ & g_\omega(\rho_{sat}),\ b_\omega, \\ & a_\rho, \\ & a_\pi, \end{aligned} \tag{2}$$

that are adjusted in a fit to experimental masses of 12 spherical nuclei (^{16}O, ^{40}Ca, ^{48}Ca, ^{56}Ni, ^{68}Ni, ^{90}Zr, ^{116}Sn, ^{132}Sn, ^{182}Pb, ^{194}Pb, ^{208}Pb, and ^{214}Pb), as well as to nuclear matter properties (saturation point, incompressibility modulus K_∞, and symmetry energy at saturation J).

The single-nucleon Dirac equation is derived by variation of the Lagrangian (1) with respect to $\bar{\psi}$,

$$[i\gamma^\mu\partial_\mu - M - \Sigma]\psi(x) = 0, \tag{3}$$

where Σ stands for the nucleon self-energy. When the variation is taken with respect to the boson fields, a set of inhomogeneous Klein-Gordon equations is obtained:

$$\left(\Box + m_\sigma^2\right)\sigma = -g_\sigma\bar{\psi}\psi, \tag{4}$$

$$\left(\Box + m_\omega^2\right)\omega^\mu = g_\omega\bar{\psi}\gamma^\mu\psi, \tag{5}$$

$$\left(\Box + m_\rho^2\right)\vec{\rho}^\mu = g_\rho\bar{\psi}\gamma^\mu\vec{\tau}\psi, \tag{6}$$

$$\left(\Box + m_\pi^2\right)\vec{\pi} = \frac{f_\pi}{m_\pi}\partial_\mu[\bar{\psi}\gamma^5\gamma^\mu\vec{\tau}\psi], \tag{7}$$

$$\Box A^\mu = e\bar{\psi}\gamma^\mu\frac{1-\tau_3}{2}\psi, \tag{8}$$

where the conservation of the baryonic current $j^\mu = \bar{\psi}\gamma^\mu\psi$ and the Coulomb gauge choice ($\partial_\mu A^\mu = 0$) have been taken into account. The Hamiltonian of the model is derived from a Legendre transformation of the Lagrangian:

$$\begin{aligned} H = & \int d^3x\ \bar{\psi}[-i\cdot\nabla + M]\psi \\ & + \frac{1}{2}\int d^3x\ \bar{\psi}\left[g_\sigma\sigma + g_\omega\gamma_\mu\omega^\mu + g_\rho\gamma_\mu\vec{\rho}^\mu\cdot\vec{\tau}\right. \\ & \left. + \frac{f_\pi}{m_\pi}\gamma_5\gamma\cdot\nabla\vec{\pi}\cdot\vec{\tau} + e\gamma_\mu A^\mu\frac{1-\tau_3}{2}\right]\psi\ . \end{aligned} \tag{9}$$

2. Inclusion of the Fock term

To explicitly include the exchange contributions, it is convenient to eliminate the mesonic degrees of freedom in Eq. (9) using the formal solution of the Klein-Gordon equations [Eq. (4)]:

$$\begin{aligned} H = & \int d^3x\ \bar{\psi}\left[-i\gamma\cdot\nabla + M\right]\psi \\ & + \frac{1}{2}\int d^3x\ d^4y\ \bar{\psi}(x)\bar{\psi}(y)\Gamma_m(x,y)D_m(x,y)\,\psi(y)\psi(x), \end{aligned} \tag{10}$$

where a summation over the repeated index $m = \{\sigma, \omega, \rho, \pi, A\}$ is implied. $D_m(x, y)$ represents the propagator of the boson m, whereas $\Gamma_m(x, y)$ corresponds to two-body interaction matrices [7]. The nucleon field is quantized, and the *no-sea* approximation [22] is adopted for the nucleon states. The nucleon field operator ψ can be expanded on an auxiliary one-body operator basis $\{c_i, c_i^\dagger\}$:

$$\psi(x) = \sum_i \{f_i(x) e^{-i\varepsilon_i t} c_i\}, \tag{11}$$

$$\psi^\dagger(x) = \sum_i \{f_i^\dagger(x) e^{i\varepsilon_i t} c_i^\dagger\}. \tag{12}$$

The Hamiltonian (10) consequently takes the form

$$H = T + \sum_m V_m, \tag{13}$$

where

$$\begin{aligned} T &= \sum_{i,j} c_i^\dagger c_j \int d^3x\, \bar{f}_i[-i\boldsymbol{\gamma}\cdot\boldsymbol{\nabla} + M] f_j \\ V_m &= \frac{1}{2}\sum_{i,j,k,l} c_i^\dagger c_j^\dagger c_k c_l \int d^3x_1 d^3x_2\, \{\bar{f}_i(\boldsymbol{x_1})\bar{f}_j(\boldsymbol{x_2}) \\ &\quad \Gamma_m(1,2) D_m(\boldsymbol{x_1}, \boldsymbol{x_2})\ f_k(\boldsymbol{x_2}) f_l(\boldsymbol{x_1})\}. \end{aligned} \tag{14}$$

The effective internucleon interaction contained in the Hamiltonian (13) is designed to be used in the self-consistent mean-field approximation. The ground state of the nuclear many-body system is, therefore, approximated by a Slater determinant:

$$|\Phi_0\rangle = \prod_i c_i^\dagger |0\rangle, \tag{15}$$

where $|\,0\rangle$ represents the single-nucleon vacuum. The energy density functional is then obtained by taking the expectation value of the Hamiltonian (13) in the ground-state Slater determinant (15):

$$\mathcal{E}^{\rm RHF}[\rho] = \langle \Phi_0 \mid H[\rho] \mid \Phi_0\rangle. \tag{16}$$

In particular, the expectation value of the potential energy operator generates a direct and an exchange term. This RHF functional can be written in terms of the one-body density operator represented by the matrix elements $\rho_{ij} = \langle \Phi_0 \mid c_j^\dagger c_i \mid \Phi_0\rangle$:

$$\begin{aligned} \mathcal{E}^{\rm RHF}[\rho, \phi_m] &= {\rm Tr}[(-i\gamma\cdot\boldsymbol{\nabla} + M + \Gamma_m\phi_m)\rho] \\ &\quad + \frac{1}{2}{\rm Tr}[\mathcal{V}[\rho]\ \rho^\dagger \otimes \rho] \\ &\quad \pm \frac{1}{2}\int d^3x \big[(\partial_\mu\phi_m)^2 + m_m^2\big]. \end{aligned} \tag{17}$$

Here Γ_m represents the one-body vertex function [7]. The trace operator involves a summation over space-time coordinates and Dirac indices. $\mathcal{V}$ is defined by its matrix elements V_{ijkl}:

$$\begin{aligned} V_{ijkl} &= \int d^3x_1\, d^3x_2\, \bar{f}_i(x_1)\bar{f}_j(x_2)\Gamma_m(1,2) D_m(x_1, x_2) \\ &\quad \times f_k(x_2) f_l(x_1). \end{aligned} \tag{18}$$

Finally, the tensor product corresponds to

$$(\rho^\dagger \otimes \rho)_{ijkl} = \rho_{ik}^\dagger \rho_{lj}. \tag{19}$$

B. RHF equations for systems with axial symmetry

The minimization of the energy functional (17) with the constraint that the single-nucleon density matrix refers to a Slater determinant leads to the RHF equations:

$$\begin{aligned} [h[\rho], \rho] &= 0, \\ \left(-\triangle + m_m^2\right)\phi_m &= \pm {\rm Tr}\left(\Gamma_m \rho\right), \end{aligned} \tag{20}$$

where

$$h[\rho] = \frac{\delta \mathcal{E}^{\rm RHF}[\rho]}{\delta\rho}. \tag{21}$$

In coordinate space the set of equations (20) can be written as

$$\begin{aligned} &\{-i\alpha\boldsymbol{\nabla} + \beta M^*(r) + [V(r) + \Sigma^R(r)]\} f_i(r, q_i) + \mathcal{F}_i(r) \\ &\quad = \epsilon_i f_i(r, q_i), \end{aligned} \tag{22}$$

$$\begin{aligned} \left(-\triangle + m_\sigma^2\right)\sigma(r) &= -g_\sigma(\rho_v)\rho_s(r), \\ \left(-\triangle + m_\omega^2\right)\omega^0(r) &= g_\omega(\rho_v)\rho_v(r), \\ \left(-\triangle + m_\rho^2\right)\rho_3^0(r) &= g_\rho(\rho_v)\rho_{tv}(r), \\ -\triangle A^0(r) &= e\rho_c(r), \end{aligned} \tag{23}$$

where q denotes isospin projection quantum number, and $\alpha \equiv \gamma^0\gamma$, $\beta \equiv \gamma^0$ are Dirac matrices. In the Dirac equation (22):

(1) $M^* = M + S(r)$ is the Dirac effective mass.

(2) $S(r)$ and $V(r)$ are the Hartree terms, i.e., they represent the direct contribution to the nucleon self-energy:

$$S(r) = g_\sigma(\rho_v)\sigma(r), \tag{24}$$

$$V(r) = g_\omega(\rho_v)\omega^0(r) + g_\rho(\rho_v)\rho_3^0(r)\tau_3 + eA^0(r). \tag{25}$$

(3) $\Sigma^R(r)$ denotes the rearrangement contribution. It can be divided into a direct term $\Sigma_H^R(r)$ and an exchange term $\Sigma_F^R(r)$. The direct contribution to the rearrangement term reads

$$\begin{aligned} \Sigma_H^R(r) &= \frac{\partial g_\sigma}{\partial\rho_v}\rho_s(r)\sigma(r) + \frac{\partial g_\omega}{\partial\rho_v}\rho_v(r)\omega_0(r) \\ &\quad + \frac{\partial g_\rho}{\partial\rho_v}\rho_{tv}(r)\rho_0^3(r). \end{aligned} \tag{26}$$

Taking the σ meson as an example, the exchange contribution to the rearrangement term reads

$$\begin{aligned} \Sigma_F^{R,\sigma}(r) &= \sum_{k,l}\delta_{q_k,q_l}\left[\frac{\partial g_\sigma}{\partial\rho_v}\bar{f}_k(q_k) f_l(q_l)\right](r) \\ &\quad \times \int d\mathbf{r}'\{D_\sigma(r, r')[g_\sigma \bar{f}_l(q_l) f_k(q_k)](r')\}. \end{aligned} \tag{27}$$

(4) $\mathcal{F}_i(r)$ denotes the Fock terms, i.e., the exchange contribution to the nucleon self-energy. For instance, the Fock term associated to the σ meson:

$$\begin{aligned} \mathcal{F}_i^\sigma(r) &= \sum_j \delta_{q_j,q_i}\int d\mathbf{r}'\{D_\sigma(r, r') \\ &\quad \times [g_\sigma f_j(\bar{q}_j) f_i(q_i)](r')\}\beta[g_\sigma f_j](r, q_j). \end{aligned} \tag{28}$$

The sources of the inhomogeneous Klein-Gordon equations (23) read

$$\rho_s(r) = \sum_i \bar{f}_i(r) f_i(r), \tag{29}$$

$$\rho_v(r) = \sum_i f_i^\dagger(r) f_i(r), \tag{30}$$

$$\rho_{tv}(r) = \sum_i f_i^\dagger(r)\tau_3 f_i(r) = \rho_v^{\text{proton}}(r) - \rho_v^{\text{neutron}}(r), \tag{31}$$

$$\rho_c(r) = \sum_i f_i^\dagger(r)\frac{1-\tau_3}{2} f_i(r) = \rho_v^{\text{proton}}(r). \tag{32}$$

In the case of deformed nuclei characterized by axial symmetry, the label i of the single-nucleon wave function $f_i(r)$ refers to the set of quantum numbers:

$$i = (\Omega, \Pi, q), \tag{33}$$

where Ω denotes the projection of the total angular momentum on the symmetry axis, Π is the parity, and q is the isospin projection that distinguishes protons and neutrons. In cylindrical coordinates $(r_\perp, \phi, z)$ the nucleon wave function takes the form [23]

$$f_i(\boldsymbol{r}) = \frac{1}{\sqrt{2\pi}} \begin{pmatrix} F_i^+(r_\perp, z; q_i) e^{i[\Omega_i - (1/2)]\varphi} \\ F_i^-(r_\perp, z; q_i) e^{i[\Omega_i + (1/2)]\varphi} \\ i G_i^+(r_\perp, z; q_i) e^{i[\Omega_i - (1/2)]\varphi} \\ i G_i^-(r_\perp, z; q_i) e^{i[\Omega_i + (1/2)]\varphi} \end{pmatrix}. \tag{34}$$

The RHF equations are solved by expanding the nucleon spinors and meson fields in the basis of a deformed harmonic oscillator. The eigenfunctions $\Phi_\alpha(r)$, $\alpha = \{n_z, n_r, m_l, m_s\}$ of the deformed harmonic oscillator potential

$$V_{\text{osc}}(r_\perp, z) = \tfrac{1}{2} M\omega_\perp^2 r_\perp^2 + \tfrac{1}{2} M\omega_z^2 z^2 \tag{35}$$

are expressed in terms of Laguerre and Hermite polynomials. They form a basis on which the nucleon wave functions $f_i(r)$ are expanded [23]:

$$\begin{aligned} F_i(r, q_i) &= \frac{1}{\sqrt{2\pi}} \begin{pmatrix} F_i^+(r_\perp, z; q_i) e^{i[\Omega_i - (1/2)]\varphi} \\ F_i^-(r_\perp, z; q_i) e^{i[\Omega_i + (1/2)]\varphi} \end{pmatrix} \\ &= \sum_\alpha f_\alpha^{(i)}(q_i)\phi_\alpha(r_\perp, z, \varphi), \end{aligned} \tag{36}$$

$$\begin{aligned} G_i(r, q_i) &= \frac{1}{\sqrt{2\pi}} \begin{pmatrix} G_i^+(r_\perp, z; q_i) e^{i[\Omega_i - (1/2)]\varphi} \\ G_i^-(r_\perp, z; q_i) e^{i[\Omega_i + (1/2)]\varphi} \end{pmatrix} \\ &= \sum_{\tilde{\alpha}} g_{\tilde{\alpha}}^{(i)}(q_i)\phi_{\tilde{\alpha}}(r_\perp, z, \varphi). \end{aligned} \tag{37}$$

In a deformed harmonic oscillator basis, therefore, the solution of the Dirac equation (22) corresponds to a diagonalization of the matrix:

$$\begin{pmatrix} A_{\alpha,\alpha'} & B_{\alpha,\tilde{\alpha}'} \\ B_{\tilde{\alpha},\alpha'} & C_{\tilde{\alpha},\tilde{\alpha}'} \end{pmatrix} \begin{pmatrix} f_{\alpha'}^{(i)}(q_i) \\ g_{\tilde{\alpha}'}^{(i)}(q_i) \end{pmatrix} = \varepsilon_i \begin{pmatrix} f_\alpha^{(i)}(q_i) \\ g_{\tilde{\alpha}}^{(i)}(q_i) \end{pmatrix}. \tag{38}$$

Detailed expressions for the Fock contribution to the matrices A, B, and C are given in Appendix A.

C. Pairing correlations

For a quantitative analysis of open-shell nuclei, both spherical and deformed, it is necessary to consider also pairing correlations. The nucleonic pairing is treated in the context of the Bogoliubov framework [24]. The resulting RHFB model provides a unified description of particle-hole (ph) and particle-particle (pp) correlations on a mean-field level by using two average potentials: the self-consistent mean field that encloses all the long-range ph correlations and a pairing field $\hat{\Delta}$ which sums up the pp correlations. Pairing correlations in nuclei are restricted to an energy window of a few MeV around the Fermi level, and their scale is well separated from the scale of binding energies, which are in the range of several hundred to a thousand MeV. There is no empirical evidence for any relativistic effect in the nuclear pairing field $\hat{\Delta}$ and, therefore, a hybrid RHFB model with a nonrelativistic pairing interaction can be formulated. Similar to most applications of the RHB model [3], the central part of the Gogny force [25] will be employed in the particle-particle (pp) channel:

$$\begin{aligned} V^{pp}(1,2) = &\sum_{i=1,2} e^{-[(\mathbf{r}_1 - \mathbf{r}_2)/\mu_i]^2} \\ &\times (W_i + B_i P^\sigma - H_i P^\tau - M_i P^\sigma P^\tau), \end{aligned} \tag{39}$$

with the set D1S [26] for the parameters μ_i, W_i, B_i, H_i, and M_i $(i = 1, 2)$. A basic advantage of the Gogny force is the finite range, which automatically guarantees a proper cutoff in momentum space.

III. RESULTS AND DISCUSSION

The explicit treatment of exchange contributions requires the calculation of nonseparable two-dimensional integrals $I_{\alpha\beta\beta'\alpha'}$ in momentum space (cf. Appendix A). These integrals involve a boson propagator and the functions $Q_{\alpha,\beta}$ [Eq. (A12)]. The Q functions are nonseparable two-dimensional spatial integrals. Their numerical evaluation imposes considerable constraints on the size of the basis of a deformed harmonic oscillator. We have verified that a RHFBz calculation with six fermionic shells yields reliable results for ground-state properties of nuclei up to $Z = 30$ (zinc isotopic chain). Various ground-state quantities (mass, axial deformation parameter, charge radius, chemical potential, single-particle energies, etc.) obtained from an expansion of the nucleon wave functions in a basis of six oscillator shells, agree within 1% from those calculated with an expansion in eight shells. Figure 1 displays the binding energy of the deformed ^{20}Ne nucleus with respect to the number of fermionic shells calculated with the PKO2, DDME2, and Gogny D1S effective interactions. The $N_{\text{shell}} = 4$ calculation is unphysical but emphasizes the similar qualitative evolution of both PKO2 and DDME2 binding energies with the number of shells up to $N_{\text{shell}} = 8$. We estimate a 1% numerical error for the PKO2 observables obtained from a six shell calculation, as seen in Fig. 1. We have also compared the results for ^{16}O and ^{40}Ca calculated with the expansion in six oscillator shells to those obtained by solving the spherical RHF equations in coordinate space, discretized on a mesh of $R_{\max} = 20$ fm and with a step $a = 0.1$ fm [12].

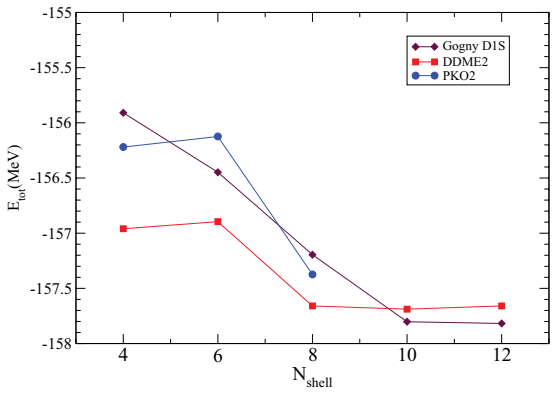

FIG. 1. (Color online) Evolution of the calculated binding energy of the ^{20}Ne nucleus with the number of major shell. The theoretical values are obtained with the PKO2 [18,19], DDME2 [3], and Gogny D1S [27] effective interactions.

The corresponding ground-state quantities and single-particle energies display relative variations of less than 1%, validating the choice of six fermionic shells for model calculation of light nuclei. The results shown hereafter correspond to calculations with 6 fermionic shells for the RHFB model and 12 fermionic shells for the RHB model.An expansion in 20 oscillator shells is used for the solution of the Klein-Gordon equations in the mesonic sector for both RHFB and RHB models.

A. Ground-state observables

This section presents results of the first application of the RHFBz model in the calculation of ground-state properties of carbon, neon, and magnesium nuclei. Masses, radii, and shapes are fundamental characteristics of nuclei and their description presents a basic test of any model and effective force. Therefore, the RHFBz model with the PKO2 and PKO3 effective interactions [18,19] in the particle-hole channel, and the central part of the Gogny D1S force [26] in the particle-particle channel, are used to calculate densities, masses, two-neutron drip lines, deformations, and charge radii of the $Z = 6, 10, 12$ isotopic chains. The PKO2 parametrization corresponds to a covariant EDF that does not explicitly include the pion field. Thus, the effects of the one-pion exchange is taken into account implicitly through the fit of the model parameters to data. PKO3 parametrizes a covariant EDF that explicitly includes the pion degree of freedom. Neither PKO2 nor PKO3 include the tensor ρ-nucleon coupling. The values of the PKO2 and PKO3 parameters are listed in Table I, together with those of one of the most successful RMF functionals: DD-ME2 [28], which has extensively been used in applications of the RHB model. In this section, to make a first study of the influence of the Fock term on a similar ground, we compare RHFBz results obtained without the inclusion of the pion field (PKO2 effective interaction) with those of the axial RHB model (DD-ME2 effective interaction).

Figures 2 and 3 compare the proton and neutron densities of neon isotopes calculated with the PKO2 and DD-ME2 effective interactions. It appears that both models predict rather similar shapes for nuclei with $A \leqslant 26$, whereas for heavier

TABLE I. Parameters of the PKO2, PKO3 [18,19], and DD-ME2 [28] effective interactions.

	PKO2	PKO3	DD-ME2
m_σ (MeV)	534.461792	525.667664	555.1238
m_ω (MeV)	783.000000	783.000000	783.0000
m_ρ (MeV)	769.000000	769.000000	769.0000
$g_\sigma(\rho_{\rm sat})$	8.920597	8.895635	10.5396
$g_\omega(\rho_{\rm sat})$	10.550553	10.802690	13.0189
$g_\rho(\rho_{\rm sat})$	2.163268	2.030285	3.6836
$f_\pi(0)$	0.000000	1.000000	0.0000
a_σ	1.375772	1.244635	1.3881
b_σ	2.064391	1.566659	1.0943
c_σ	3.052417	2.074581	1.7057
d_σ	0.330459	0.400843	0.4421
a_ω	1.451420	1.245714	1.3892
b_ω	3.574373	1.645754	0.9240
c_ω	5.478373	2.177077	1.4620
d_ω	0.246668	0.391293	0.4775
a_ρ	0.631605	0.635336	0.5647
a_π	0.000000	0.934122	0.0000

Ne isotopes larger deformations are calculated with the RHB model with DD-ME2, especially for proton densities.

In Fig. 4 we display the absolute deviations of the calculated binding energies from the experimental values of neon isotopes for the two relativistic effective interactions PKO2, DD-ME2, the Gogny force D1S, and the Skyrme interaction SLy4. Positive deviations correspond to underbound nuclei. One might notice that deformed RHFB calculations with PKO2 predict binding energies with a level of agreement with data comparable to that of the Gogny D1S force and, for heavier isotopes, slightly better than RHB with DD-ME2. Much larger deviations from data are calculated with the Skyrme force SLy4. Similar results are found in the carbon and magnesium isotopic chains. This is quantified in Table II, where we compare the root-mean-square deviations of theoretical binding energies for the $Z = 6, 10, 12$ isotopic chains. PKO2 predictions are closest to the experimental values in the neon

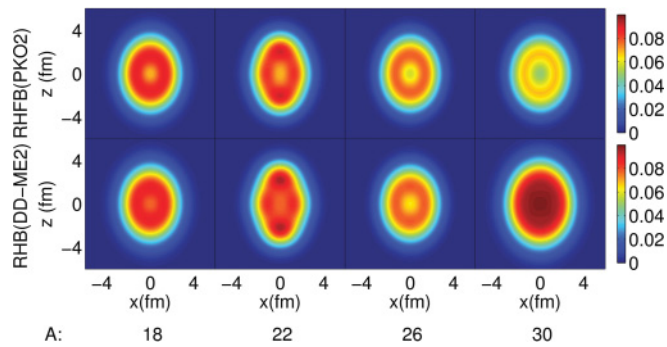

FIG. 2. (Color online) Proton density in the Ne isotopic chain. The single-nucleon densities calculated with the PKO2 (RHFBz) and DD-ME2 (RHB) effective interactions are plotted in the (Oxz) plan with $x, z \in [-6\ \text{fm}, 6\ \text{fm}]$. The color code denotes densities in the interval $\left[0\ \text{fm}^{-3}, 0.09\ \text{fm}^{-3}\right]$.

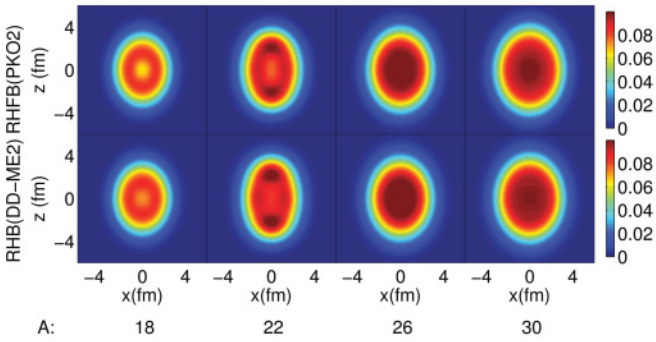

FIG. 3. (Color online) Same as Fig. 2 for neutron density in the interval [0 fm^{-3}, 0.1 fm^{-3}].

and magnesium isotopic chains, whereas DD-ME2 gives the smallest rms deviation for carbon nuclei.

The two-neutron separation energy $S_{2n} \equiv E_{\rm tot}(Z,N) - E_{\rm tot}(Z,N-2)$ of Mg isotopes, calculated with PKO2 and DD-ME2, are compared to data in Fig. 5. In general, the RHFBz results obtained with the PKO2 parameter set are closer to the experimental two-neutron separation energies. The last two-neutron bound Mg nucleus is ^{38}Mg in the RHFBz calculation with PKO2, whereas the RHB model with DD-ME2 predicts ^{40}Mg to be the last bound isotope. Compared to DD-ME2, the PKO2 two-neutron separation energies are also found closer to data in the carbon and neon isotopic chains.

The evolution of the axial deformation parameter β with mass number along the carbon isotopic chain is displayed in Fig. 6. No experimental results extracted from $B(E2)$ measurements are presented insofar as it is not adequate to directly compare the static deformation parameter from the dynamical one extracted from the experiment, in such light even-even nuclei. PKO2 and Skyrme SLy4 predict deformations that are systematically smaller than those obtained with the DD-ME2 and Gogny D1S interactions, or with the Skyrme SGII effective force. In particular, PKO2 and SLy4 predict basically spherical

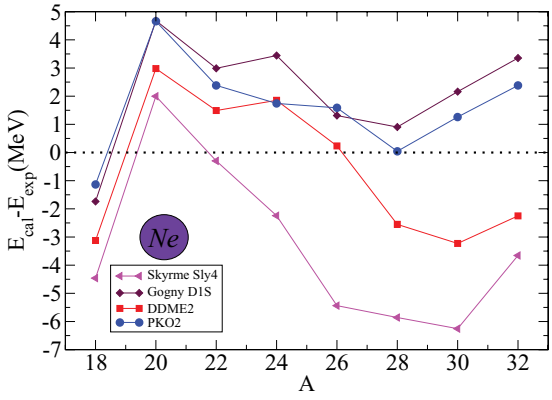

FIG. 4. (Color online) Absolute deviations of the calculated binding energies from the experimental values of the Ne isotopic chain. The theoretical values are obtained with the PKO2 [18,19], DDME2 [3], Gogny D1S [27], and Skyrme SLy4 [29] effective interactions. The data are from Ref. [30]. For ^{32}Ne the calculated values are compared to the extrapolated binding energy.

TABLE II. Root-mean-square deviations from experimental data of binding energies calculated with the PKO2 [18,19], DD-ME2 [3], Gogny D1S [27], and Skyrme SLy4 [29] effective interactions from for the carbon, neon, and magnesium isotopic chains.

	PKO2	DDME2	Gogny D1S	Skyrme SLy4
$\sigma_{\rm C}$ (MeV)	2.144	1.443	3.185	2.874
$\sigma_{\rm Ne}$ (MeV)	2.263	2.429	2.750	4.342
$\sigma_{\rm Mg}$ (MeV)	2.480	2.582	3.337	3.269

shapes between ^{10}C and ^{16}C whereas, except for ^{14}C, rather large ground-state deformations are calculated with the other three interactions. The case of ^{16}C is particularly interesting. Early experiments at Riken indicated an anomalously small $B(E2)$ [32], and a strong prolate deformation [33]. Therefore, the nucleus ^{16}C was thought to be characterized by valence neutrons decoupled from a quasispherical core. Different models corroborated these results (see, for instance, [34]). Recent measurements of $B(E2; 2_1^+ \rightarrow 0^+)$ in ^{16}C gave a value that is more consistent with what is observed in nuclei with similar N/Z [35,36]. The current result does not support the description of ^{16}C in terms of valence neutrons decoupled from the spherical core. The RHFBz model calculation with the PKO2 interaction, in particular, predicts the neutron and proton axial deformations in ^{16}C: $\beta_n = 0.08$ and $\beta_p = 0.06$, respectively.

The charge radii of neon isotopes, calculated with PKO2 and DD-ME2, are shown in comparison with data in Fig. 7. In lighter Ne nuclei the theoretical values predicted by the RHB model with DD-ME2 are in much better agreement with experiment, whereas for $A \geqslant 26$ both models yield similar charge radii. It should be noted that contrary to DD-ME2, PKO2 does not include the charge radii in its fit to spherical nuclei.

Structure models can also be compared by considering the corresponding single-nucleon spectra. In Ref. [19] the predictions of the spherical RHF model were tested in comparison to data for ^{16}O and ^{40}Ca. In Fig. 8 we compare the proton Nilsson orbitals of ^{28}Mg, calculated with PKO2

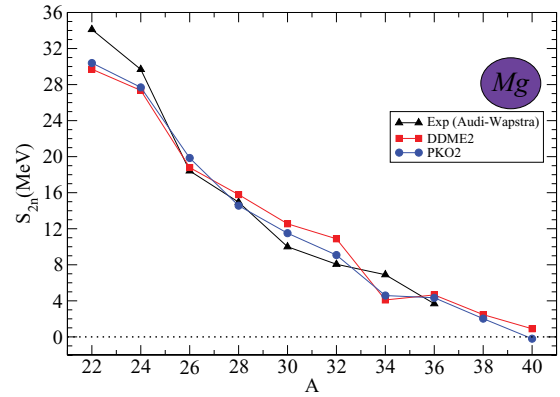

FIG. 5. (Color online) Two-neutron separation energy in the magnesium isotopic chain. The relativistic mean-field results: RHFBz with PKO2 [18,19] and RHB with DD-ME2 [28], are compared to data (Audi-Wapstra [30]).

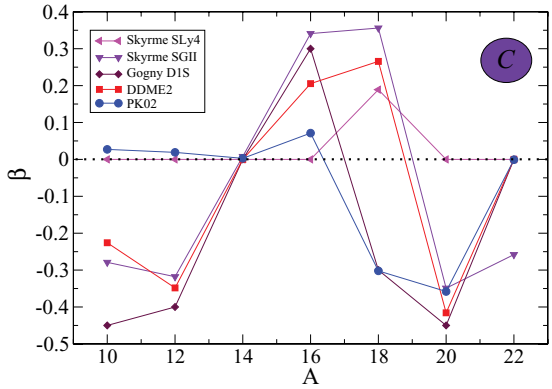

FIG. 6. (Color online) Axial deformation parameter β of C nuclei as a function of the mass number. The calculated values correspond to the PKO2 [18,19], DD-ME2 [28], Gogny D1S, Skyrme SLy4, and Skyrme SGII [31] effective interactions.

and DD-ME2. Although the ordering of Nilsson states is the same for both interactions, in general the density of states around the Fermi level is larger when calculated with the RHFBz approach. This originates from the larger effective nucleon mass characterizing the PKO2 interaction compared to the DDME2 one. Namely, the density of states depends on the effective mass [38], which is increased by the spatial nonlocality of the mean-field potential (Fock terms).

B. The PKO2 versus PKO3 parametrization

In the framework of shell-model calculations the tensor contribution, arising from pion exchange, has been found to play an important role in the description of the evolution of shell structures with proton/neutron numbers [15]. The effect of including the pion field in the RHBz model can be analyzed using the PKO3 effective interaction [18,19]. In the relativistic mean-field framework the pseudovector coupling of the pion to the nucleon generates part of the tensor contribution to the effective internucleon interaction, the remaining part being in-

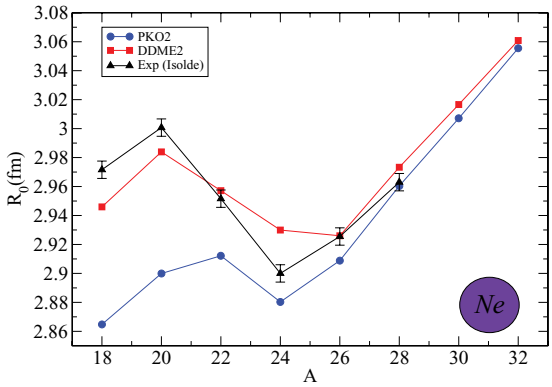

FIG. 7. (Color online) Charge radii in the neon isotopic chain. The theoretical values calculated with PKO2 [18,19] and DD-ME2 [28] are compared to the ISOLDE experimental values [37].The error bars do not include the atomic factor and therefore should be increased by 10%.

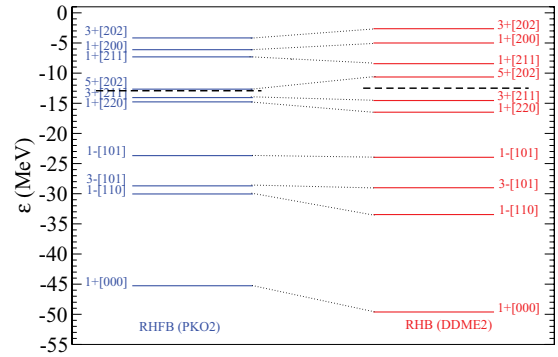

FIG. 8. (Color online) Comparison of the single-proton levels of ^{28}Mg, calculated with the PKO2 [18,19] and DD-ME2 [28] effective interactions. The levels are labeled by Nilsson quantum numbers. The dashed line denotes the chemical potential.

duced by the tensor ρ-nucleon coupling. Here we consider the differences between the PKO2 and PKO3 parametrizations on binding energies, ground-state axial deformation parameters, and charge radii. Contrary to the PKO2 effective interaction, the PKO3 effective interaction explicitly includes the pion contribution during the fit to data. The other parameters of the Lagrangian are also affected (Table I), meaning that the inclusion of the pseudovector $\pi - N$ coupling alters how correlations beyond mean field are implicitly taken into account through the effective meson couplings.

Figure 9 displays the absolute deviations of the theoretical binding energies from data for the sequence of neon isotopes. In addition to the results shown in Fig. 4, here we also include the deviations obtained in the RHFBz calculation with the PKO3 interaction. The PKO3 results for the ^{18}Ne, ^{26}Ne, ^{28}Ne, and ^{30}Ne are on the same level of accuracy or better than those obtained with PKO2, i.e., without the explicit inclusion of the pion field, whereas they show less agreement with data for the other Ne nuclei.

The evolution of the axial deformation parameter β in the neon isotopic chain is illustrated in Fig. 10. In general, the deformation predicted by PKO3 is larger than that calculated with PKO2 and, therefore, closer to the results obtained with the DD-ME2 and Gogny D1S effective interactions. PKO3

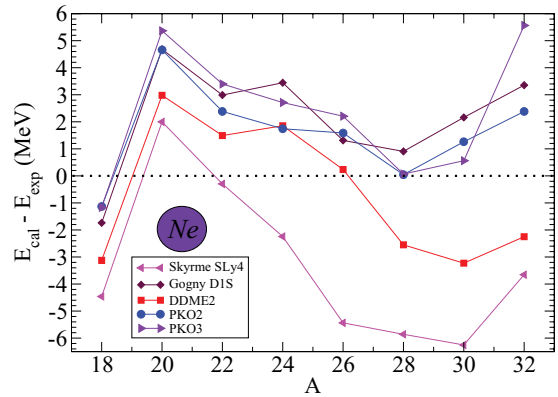

FIG. 9. (Color online) Same as in Fig. 4, but with the PKO3 RHFBz calculation in addition.

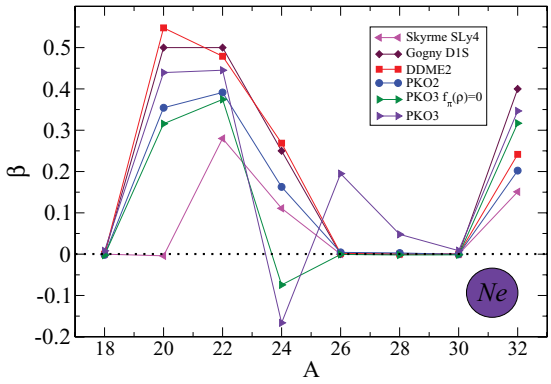

FIG. 10. (Color online) Same as in Fig. 6, except for the neon isotopic chain, and with the PKO3 RHFBz calculations and the PKO3 RHFBz results with $f_\pi(\rho)$ sets to 0 in addition.

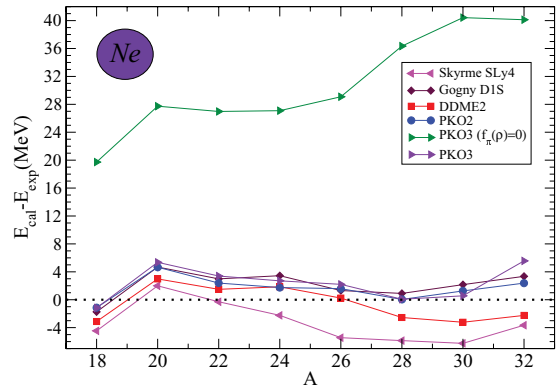

FIG. 12. (Color online) Same as in Fig. 9, but with the PKO3 RHFBz calculation with $f_\pi(\rho) = 0$ in addition.

predicts an oblate shape for ^{24}Ne (quasidegenerate in energy with a prolate solution at $\beta = 0.3$), whereas a prolate ground-state shape for this nucleus is obtained with PKO2, DDME2, Gogny D1S (quasidegenerate in energy with an oblate solution at $\beta = -0.15$), and Skyrme SLy4 interactions. Moreover, all these interactions, except PKO3 that predicts a prolate ground state, give no deformation for ^{26}Ne and ^{28}Ne.

Finally, in Fig. 11 we illustrate the differences between the PKO2 and PKO3 parametrizations on the calculated charge radii of neon isotopes. The results obtained with PKO3 are shown in comparison with the ISOLDE data [37] and with theoretical values predicted by the DD-ME2 (RHB) and PKO2 (RHFBz) effective interactions (cf. also Fig. 7). One might notice that the explicit inclusion of the pion contribution leads to an enhancement of the calculated charge radii as compared with the values obtained with PKO2, bringing them closer to the predictions of DD-ME2 and, for the lighter isotopes, in better agreement with data.

C. The effect of including the pion field

In order to isolate the effect of the pseudovector $\pi - N$ coupling on the observables, we compare calculations based on the PKO3 effective interaction where the pion contribution

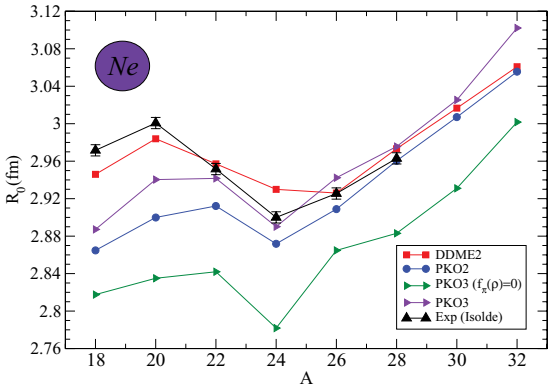

FIG. 11. (Color online) Same as in Fig. 7, but with the PKO3 RHFBz calculation in addition.

is switched on and off. Figure 12 displays the absolute deviations of the theoretical binding energies from data for the sequence of neon isotopes. In addition to the results shown in Fig. 9, here we also include the deviations obtained in the RHFBz calculation with the PKO3 interaction where the pion contribution is switched off. Switching on the pion coupling constant brings relevant binding to the neon isotopes.

In Fig. 10 the comparison between the PKO3 curve and the PKO3 one where the pion coupling is set to zero shows that the prolate shape of ^{26,28}Ne is driven by the pion, whereas interactions without the explicit tensor term predict a spherical shape. The effect of the pion field on single-nucleon spectra is illustrated in Figs. 13 and 14, where we display the proton and neutron single-particle levels in ^{26}Ne obtained in RHFBz calculations with the PKO3 effective interaction where the pion coupling is switched on and off. PKO3 with the pion coupling set to zero yields a spherical ground-state shape and the Nilsson levels are degenerate; in contrast the degeneracy is lifted in the calculation performed with the complete PKO3 interaction. Here one notices a clear signature of the effect

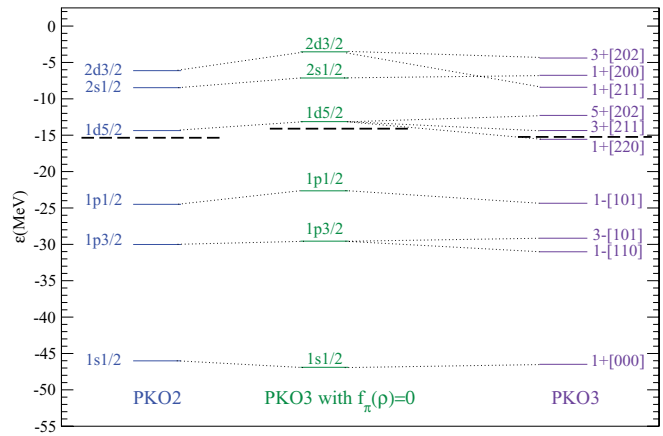

FIG. 13. (Color online) Comparison of the single-proton levels of ^{26}Ne, calculated with the PKO2 effective interaction (on the left), the PKO3 effective interaction where the pion coupling is switched on (on the right), and that where it is switched off (in the middle). The dashed line denotes the chemical potential.

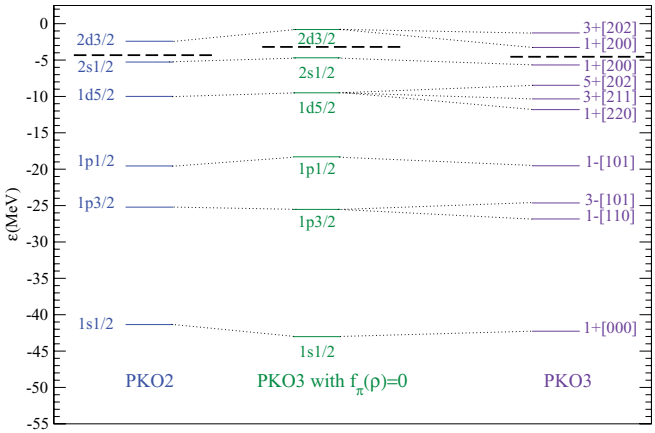

FIG. 14. (Color online) Same as in Fig. 13, but for the neutron single-particle levels.

of the pion on single-nucleon spectra and the corresponding evolution of shell structures.

In Fig. 11 we illustrate the effect of including the pion field on the calculated charge radii of neon isotopes. Switching on the pion coupling constant results in a drastic enhancement of the neon isotope charge radii.

IV. CONCLUSION

We have developed the relativistic Hartree-Fock-Bogoliubov model for axially deformed nuclei (RHFBz). An effective Lagrangian with density-dependent meson-nucleon couplings is used in the particle-hole channel and the central part of the Gogny force in the particle-particle channel. The RHFBz quasiparticle equations are solved by expansion in the basis of a deformed harmonic oscillator potential. The numerical complexity brought by the explicit treatment of the Fock term within relativistic mean-field theory limits, at present, the size of the oscillator basis for the expansion of the nucleon wave functions. The current version of the model provides a reliable and numerically stable description of ground-state properties up to the zinc isotopic chain. Further numerical optimization is possible and work is in progress to extend the size of the deformed oscillator basis to 12 fermionic shells, allowing a description of medium-mass and heavy nuclei. In this work illustrative RHFBz calculations have been performed for carbon, neon, and magnesium isotopes. Results obtained with the RHF effective force PKO2 have been compared to experimental masses and charge radii and, in addition, ground-state deformation and single-nucleon spectra have been shown in comparison with the predictions of one of the most successful RMF meson-exchange interactions: DD-ME2, as well as with the results calculated with the nonrelativistic Gogny D1S and Skyrme SLy4 interactions. The effect of explicitly including the pion field has been investigated for binding energies, deformation parameters, and charge radii. The addition of the tensor ρ-nucleon coupling will complete the model and thus enable studies of the role of tensor components of the effective internucleon interaction in the evolution of shell structures in deformed nuclei.

ACKNOWLEDGMENTS

The authors acknowledge fruitful discussions with M. Grasso, M. Kowalka, H. Liang, D. Lunney, T. Nikšić, P. Ring, N. V. Giai, and D. Verney. This work was supported in part by the ANR Nexen and MZOSProject No. 1191005-1010.

APPENDIX : EXPLICIT EXPRESSIONS FOR THE EXCHANGE CONTRIBUTION

Each matrix A, B, and C in Eq. (38) contains the kinetic, direct, exchange, and rearrangement contributions. The explicit expressions for the kinetic and direct contributions read

$$\begin{aligned}\begin{pmatrix} A_{\alpha,\alpha'} \\ C_{\alpha,\alpha'} \end{pmatrix} &= \delta_{m_l,m_l'}\delta_{m_s,m_s'} N_{n_r}^{ml} N_{n_z} N_{n_r'}^{ml'} N_{n_z'} \\ &\times \int_0^\infty d^\eta e^{-\eta} \eta^{m_l} L_{n_r}^{ml}(\eta) L_{n_r'}^{ml'}(\eta) \\ &\times \int_0^\infty d^\zeta e^{-\zeta^2} H_{n_z}(\zeta) H_{n_z'}(\zeta) \\ &\times [M^*(b\perp\sqrt{\eta}, b_z\zeta) \pm V(b\perp\sqrt{\eta}, b_z\zeta)], \end{aligned} \tag{A1}$$

$$\begin{aligned} B_{\alpha,\alpha'} &= \delta_{m_l,m_l'}\delta_{m_s,m_s'}\delta_{n_r,n_r'} \frac{(-1)^{-m_s+(1/2)}}{b_z} \\ &\times \left(\delta_{n_z',n_z+1}\sqrt{\frac{n_z'}{2}} - \delta_{n_z,n_z'+1}\sqrt{\frac{n_z}{2}} \right) \\ &+ \delta_{m_l,m_l'}\delta_{n_z,n_z'} \frac{N_{n_r}^{ml} N_{n_r'}^{ml'}}{b_\perp} \\ &\times \left\{ \delta_{m_s',m_s+1} \int_0^\infty d^\eta e^{-\eta} \eta^{m_l-(1/2)} L_{n_r}^{ml}(\eta) \right. \\ &\times \left[\tilde{L}_{n_r'}^{ml}(\eta) + (1-m_l) L_{n_r'}^{ml}(\eta) \right] \\ &+ \delta_{m_s,m_s'+1} \int_0^\infty d^\eta e^{-\eta} \eta^{m_l-(1/2)} L_{n_r}^{ml}(\eta) \\ &\times \left. \left[\tilde{L}_{n_r'}^{ml}(\eta) + (1+m_l) L_{n_r'}^{ml}(\eta) \right] \right\}, \end{aligned} \tag{A2}$$

where

$$\tilde{L}_{n_r}^{ml}(\eta) = (2m_l + n_r - \eta) L_{n_r}^{ml}(\eta) - 2(n_r + m_l) L_{n_r-1}^{ml}(\eta). \tag{A3}$$

Taking the σ meson as an example, the exchange contribution to the A, B, and C matrices is given by the following expressions:

$$\begin{aligned} A_{\alpha,\alpha'}^{\sigma}(q_i) = \sum_{j>0} \delta_{q_j,q_i} \sum_{\beta,\beta'} f_\beta^{(j)}(q_j) f_{\beta'}^{(j)}(q_j) \Big\{ & \delta_{m_{s_{\beta'\alpha'}}}^{\parallel} \delta_{m_{s_{\beta\alpha}}}^{\parallel} I_{\alpha\beta\beta'\alpha'}^{\sigma} \\ & + \delta_{m_{s_{\beta'\alpha'}},0}^{\nparallel} \delta_{m_{s_{\beta\alpha}}}^{\nparallel} (2ms_\beta)(2ms_{\beta'}) \check{I}_{\alpha\beta\beta'\alpha'}^{\sigma} \Big\}, \end{aligned} \tag{A4}$$

$$\begin{aligned} B_{\alpha,\tilde{\alpha}'}^{\sigma}(q_i) = -\sum_{j>0} \delta_{q_j,q_i} \sum_{\beta,\tilde{\beta}'} f_\beta^{(j)}(q_j) g_{\tilde{\beta}'}^{(j)}(q_j) \Big\{ & \delta_{m_{s_{\tilde{\beta}'\tilde{\alpha}'}}}^{\parallel} \delta_{m_{s_{\beta\alpha}}}^{\parallel} I_{\alpha\beta\tilde{\beta}'\tilde{\alpha}'}^{\sigma} \\ & - \delta_{m_{s_{\tilde{\beta}'\tilde{\alpha}'}}}^{\nparallel} \delta_{m_{s_{\beta\alpha}}}^{\nparallel} (2ms_\beta)(2ms_{\tilde{\beta}'}) \check{I}_{\alpha\beta\tilde{\beta}'\tilde{\alpha}'}^{\sigma} \Big\}, \end{aligned} \tag{A5}$$

$$C^{\sigma}_{\tilde{\alpha},\tilde{\alpha'}}(q_i) = \sum_{j>0}\delta_{q_j,q_i}\sum_{\tilde{\beta},\tilde{\beta'}} g^{(j)}_{\tilde{\beta}}(q_j)g^{(j)}_{\tilde{\beta'}}(q_j)\Big\{\delta^{\parallel}_{m_{s_{\tilde{\beta'}\tilde{\alpha'}}}}\delta^{\parallel}_{m_{s_{\tilde{\beta}\tilde{\alpha}}}} I^{\sigma}_{\tilde{\alpha}\tilde{\beta}\tilde{\beta'}\tilde{\alpha'}} + \delta^{\nparallel}_{m_{s_{\tilde{\beta'}\tilde{\alpha'}}}}\delta^{\nparallel}_{m_{s_{\tilde{\beta}\tilde{\alpha}}}}(2ms_{\tilde{\beta}})(2ms_{\tilde{\beta'}})\check{I}^{\sigma}_{\tilde{\alpha}\tilde{\beta}\tilde{\beta'}\tilde{\alpha'}}\Big\}, \quad \text{(A6)}$$

where

$$\delta^{\parallel}_{m_{s_{\beta\alpha}}} \equiv \delta_{m_{s_\beta},m_{s_\alpha}}, \quad \text{(A7)}$$

$$\delta^{\nparallel}_{m_{s_{\beta\alpha}}} \equiv \delta_{m_{s_\beta},-m_{s_\alpha}}, \quad \text{(A8)}$$

$$I^{\sigma}_{\alpha\beta\beta'\alpha'} \equiv \int d\mathbf{r}[g_\sigma\phi^*_\alpha\phi_\beta](r)\int d\mathbf{r}'\, D_\sigma(r,r')[g_\sigma\phi^*_{\beta'}\phi_{\alpha'}](r'), \quad \text{(A9)}$$

$$\check{I}^{\sigma}_{\alpha\beta\beta'\alpha'} \equiv \int d\mathbf{r}[g_\sigma\phi^*_\alpha\phi^*_\beta](r)\int d\mathbf{r}'\, D_\sigma(r,r')[g_\sigma\phi_{\beta'}\phi_{\alpha'}](r'). \quad \text{(A10)}$$

The Fock terms are characterized by nondegenerate contributions to the positive and negative Ω_j blocks. The integrals can be written as

$$I^{m}_{\alpha\beta\beta'\alpha'} = (-1)^{(m_{l_{\alpha'}}-m_{l_{\beta'}})}\delta_{(m_{l_\beta}-m_{l_\alpha})+(m_{l_{\alpha'}}-m_{l_{\beta'}}),0} \times\int\frac{dk_\perp\,dk_z}{(2\pi)^2}Q_{\alpha,\beta}(k_\perp,k_z)\frac{k_\perp}{k^2_\perp+k^2_z+m^2_m} \times Q_{\beta',\alpha'}(k_\perp,-k_z), \quad \text{(A11)}$$

where

$$Q_{\alpha,\beta}(k_\perp,k_z) = \int dr_{1\perp}\,dz_1\,r_{1\perp}[g_\sigma\check{\phi}_\alpha\check{\phi}_\beta](r_{1\perp},z_1) \times e^{ik_zz_1}J_{(m_{l_\beta}-m_{l_\alpha})}(k_\perp r_{1\perp}),$$

$$Q_{\beta',\alpha'}(k_\perp,-k_z) = \int dr_{2\perp}\,dz_2\,r_{2\perp}[g_\sigma\check{\phi}_{\beta'}\check{\phi}_{\alpha'}](r_{2\perp},z_2) \times e^{-ik_zz_2}J_{(m_{l_{\alpha'}}-m_{l_{\beta'}})}(k_\perp r_{2\perp}). \quad \text{(A12)}$$

Taking again the case of the σ meson field as an example, the exchange contribution to the rearrangement term reads

$$\Sigma^{\sigma,Ex}_R(\boldsymbol{r}) = \sum_{m,n}\delta_{q_m,q_n}\left[\frac{\partial g_\sigma}{\partial\rho_v}\bar{f}_m(q_m)f_n(q_n)\right](r) \times\int d^3r'\{D_\sigma(r,r')[g_\sigma\bar{f}_n(q_n)f_m(q_m)](r')\}. \quad \text{(A13)}$$

In the basis of a deformed oscillator, relation (A13) takes the form

$$\Sigma^{\sigma,Ex}_{R;\alpha\alpha'} = \sum_{m>0}\sum_{\mu\mu'}f^{(m)}_\mu(q_m)f^{(m)}_{\mu'}(q_m)\tilde{A}^{\sigma}_{\alpha\alpha'\mu\mu'} + 2\sum_{m>0}\sum_{\tilde{\mu}\mu'}g^{(m)}_{\tilde{\mu}}(q_m)f^{(m)}_{\mu'}(q_m)\tilde{B}^{\sigma}_{\alpha\alpha'\tilde{\mu}\mu'} + \sum_{m>0}\sum_{\tilde{\mu}\tilde{\mu'}}g^{(m)}_{\tilde{\mu}}(q_m)g^{(m)}_{\tilde{\mu'}}(q_m)\tilde{C}^{\sigma}_{\alpha\alpha'\tilde{\mu}\tilde{\mu'}}. \quad \text{(A14)}$$

The matrices $\tilde{A}$, $\tilde{B}$, and $\tilde{C}$ are obtained by replacing the integrals $I^{\sigma}_{\mu\nu\nu'\mu'}$ and $\check{I}^{\sigma}_{\mu\nu\nu'\mu'}$ in the expressions for the corresponding matrices A, B, and C, with the integrals $K^{\sigma}_{\alpha\alpha'\mu\nu;\nu'\mu'}$ and $\check{K}^{\sigma}_{\alpha\alpha'\mu\nu;\nu'\mu'}$:

$$K^{m}_{\alpha,\alpha',\gamma,\lambda,\lambda',\gamma'} = \int d\mathbf{r}\left[\phi^*_\alpha\phi_{\alpha'}\frac{\partial g_m}{\partial\rho_v}\phi^*_\gamma\phi_\lambda\right](r) \times\int d\mathbf{r}'\, D_m(r,r')[g_m\phi^*_{\lambda'}\phi_{\gamma'}](r'), \quad \text{(A15)}$$

$$\check{K}^{m}_{\alpha,\alpha',\gamma,\lambda,\lambda',\gamma'} = \int d\mathbf{r}\left[\phi^*_\alpha\phi_{\alpha'}\frac{\partial g_m}{\partial\rho_v}\phi^*_\gamma\phi^*_\lambda\right](r) \times\int d\mathbf{r}'\, D_m(r,r')[g_m\phi_{\lambda'}\phi_{\gamma'}](r'). \quad \text{(A16)}$$

These integrals can be written in the form

$$K_{\alpha,\alpha',\gamma,\lambda,\lambda',\gamma'} = \delta_{(m_{l_{\alpha'}}-m_{l_\alpha}+m_{l_\lambda}-m_{l_\gamma})+(m_{l_{\gamma'}}-m_{l_{\lambda'}}),0} \times\int\frac{dk_\perp\,dk_z}{(2\pi)^2}Q_{\alpha,\alpha',\gamma,\lambda}(k_\perp,k_z)\frac{k_\perp}{k^2_\perp+k^2_z+m^2_m} \times Q_{\lambda',\gamma'}(-k_\perp,-k_z), \quad \text{(A17)}$$

where

$$Q_{\alpha,\alpha',\gamma,\lambda}(k_\perp,k_z) = \int dr_{1\perp}\,dz_1\,r_{1\perp}\left[\check{\phi}_\alpha\check{\phi}_{\alpha'}\frac{\partial g_m}{\partial\rho_v}\check{\phi}_\gamma\check{\phi}_\lambda\right](r_{1\perp},z_1) \times e^{ik_zz_1}J_{(m_{l_{\alpha'}}-m_{l_\alpha}+m_{l_\lambda}-m_{l_\gamma})}(k_\perp r_{1\perp}), \quad \text{(A18)}$$

$$Q_{\lambda',\gamma'}(-k_\perp,-k_z) = \int dr_{2\perp}\,dz_2\,r_{2\perp}[g_m\check{\phi}_{\lambda'}\check{\phi}_{\gamma'}](r_{2\perp},z_2) \times e^{-ik_zz_2}J_{(m_{l_{\gamma'}}-m_{l_{\lambda'}})}(-k_\perp r_{2\perp}), \quad \text{(A19)}$$

and

$$\check{K}_{\alpha,\alpha',\gamma,\lambda,\lambda',\gamma'} = \delta_{(m_{l_{\alpha'}}-m_{l_\alpha}-m_{l_\lambda}-m_{l_\gamma})+(m_{l_{\gamma'}}+m_{l_{\lambda'}}),0} \times\int\frac{dk_\perp\,dk_z}{(2\pi)^2}Q^{-}_{\alpha,\alpha',\gamma,\lambda}(k_\perp,k_z)\frac{k_\perp}{k^2_\perp+k^2_z+m^2_m} \times Q^{+}_{\lambda',\gamma'}(-k_\perp,-k_z), \quad \text{(A20)}$$

where

$$Q^{-}_{\alpha,\alpha',\gamma,\lambda}(k_\perp,k_z) = \int dr_{1\perp}\,dz_1\,r_{1\perp}\left[\check{\phi}_\alpha\check{\phi}_{\alpha'}\frac{\partial g_m}{\partial\rho_v}\check{\phi}_\gamma\check{\phi}_\lambda\right](r_{1\perp},z_1) \times e^{ik_zz_1}J_{(m_{l_{\alpha'}}-m_{l_\alpha}-m_{l_\lambda}-m_{l_\gamma})}(k_\perp r_{1\perp}), \quad \text{(A21)}$$

$$Q^{+}_{\lambda',\gamma'}(-k_\perp,-k_z) = \int dr_{2\perp}\,dz_2\,r_{2\perp}[g_m\check{\phi}_{\lambda'}\check{\phi}_{\gamma'}](r_{2\perp},z_2) \times e^{-ik_zz_2}J_{(m_{l_{\gamma'}}+m_{l_{\lambda'}})}(-k_\perp r_{2\perp}). \quad \text{(A22)}$$

[1] D. Lacroix, T. Duguet, and M. Bender, Phys. Rev. C **79**, 044318 (2009).
[2] M. Bender, P.-H. Heenen, and P.-G. Reinhard, Rev. Mod. Phys. **75**, 121 (2003).
[3] D. Vretenar, A. V. Afanasjev, G. A. Lalazissis, and P. Ring, Phys. Rep. **409**, 101 (2005).
[4] R. J. Furnstahl and B. D. Serot, Comments Nucl. Part. Phys. **2**, A23 (2000).
[5] A. V. Afanasjev and H. Abusara, Phys. Rev. C **81**, 014309 (2010).
[6] J. N. Ginocchio, Phys. Rep. **414**, 165 (2005).
[7] A. Bouyssy, J.-F. Mathiot, N. Van Giai, and S. Marcos, Phys. Rev. C **36**, 380 (1987).
[8] P. Bernardos, V. N. Fomenko, N. V. Giai, M. L. Quelle, S. Marcos, R. Niembro, and L. N. Savushkin, Phys. Rev. C **48**, 2665 (1993).
[9] W. H. Long, N. Van Giai, and J. Meng, Phys. Lett. B **640**, 150 (2006).
[10] W. H. Long, P. Ring, N. Van Giai, and J. Meng, Phys. Rev. C **81**, 024308 (2010).
[11] W. H. Long, H. Sagawa, J. Meng, and N. Van Giai, Europhys. Lett. **82**, 12001 (2008).
[12] W. H. Long, H. Sagawa, N. V. Giai, and J. Meng, Phys. Rev. C **76**, 034314 (2007).
[13] H. Liang, N. Van Giai, and J. Meng, Phys. Rev. Lett. **101**, 122502 (2008).
[14] H. Liang, W. H. Long, J. Meng, and N. Van Giai, Eur. Phys. J. A **44**, 119-124 (2010).
[15] T. Otsuka, T. Suzuki, R. Fujimoto, H. Grawe, and Y. Akaishi, Phys. Rev. Lett. **95**, 232502 (2005).
[16] N. Paar, T. Nikšić, D. Vretenar and P. Ring, Phys. Rev. C **69**, 054303 (2004).
[17] T. Nikšić, D. Vretenar, and P. Ring, Prog. Part. Nucl. Phys. **66**, 519 (2011).
[18] W. H. Long, N. Van Giai, and J. Meng, arXiv:nucl-th/0608009.
[19] W. H. Long, Ph.D. thesis, Université Paris-Sud 11, 2005.
[20] T. Nikšić, D. Vretenar, P. Finelli, and P. Ring, Phys. Rev. C **66**, 024306 (2002).
[21] S. Typel and H. H. Wolter, Nucl. Phys. A **656**, 331 (1999).
[22] R. J. Furnstahl, Lect. Notes Phys. **641**, 1 (2004).
[23] P. Ring, Y. K. Gambhir, and G. A. Lalazissis, Comput. Phys. Commun. **105**, 77-97 (1997).
[24] P. Ring and P. Schuck, *The Nuclear Many-Body Problem* (Springer-Verlag, Berlin, 1980).
[25] J. F. Berger, M. Girod, and D. Gogny, Nucl. Phys. A **428**, 23c (1984).
[26] J. F. Berger, M. Girod, and D. Gogny, Comput. Phys. Commun. **63**, 365 (1991).
[27] S. Hilaire and M. Girod, Eur. Phys. J. A **33**, 237-241 (2007).
[28] G. A. Lalazissis, T. Nikšić, D. Vretenar, and P. Ring, Phys. Rev. C **71**, 024312 (2005).
[29] M. V. Stoitsov, J. Dobaczewski, W. Nazarewicz, S. Pittel, and D. J. Dean, Phys. Rev. C **68**, 054312 (2003).
[30] G. Audi and W. H. Wapstra, Nucl. Phys. A **565**, 1 (1993).
[31] H. Sagawa, X. R. Zhou, X. Z. Zhang, and T. Suzuki, Phys. Rev. C **70**, 054316 (2004).
[32] N. Imai *et al.*, Phys. Rev. Lett. **92**, 062501 (2004).
[33] H. J. Ong *et al.*, Phys. Rev. C **73**, 024610 (2006).
[34] K. Hagino and H. Sagawa, Phys. Rev. C **75**, 021301 (2007).
[35] M. Wiedeking *et al.*, Phys. Rev. Lett. **100**, 152501 (2008).
[36] A. H. Wuosmaa *et al.*, Phys. Rev. Lett. **105**, 132501 (2010).
[37] K. Marinova *et al.* (submitted in Phys. Rev. C).
[38] M. Beiner*et al*, Nucl. Phys. A **238**, 29 (1975).